Journal of Statistical Physics, Vol. 76, Nos. 3/4, 1994

Correlation Dimension of the Sheared Hard-Disk Lorentz Gas

Janka Petravic,[1] Dennis J. Isbister,[1] and Gary P. Morriss[2]

Received June 15, 1993; final January 25, 1994

The correlation dimension for the isokinetic Lorentz gas is calculated for hard disks using nonequilibrium molecular dynamics simulation. The trajectories are confined to a strange attractor embedded in a four-dimensional phase space—the additional degree of freedom having not been included properly until this work. This degree of freedom accounts for the explicit time dependence of the system (as quantified by the moving periodic cells under shear) and is significant because the collisions tend to synchronize with the periodic change of symmetry of the lattice at high shear rates.

KEY WORDS: Correlation dimension; nonequilibrium molecular dynamics; shear flow; hard disks.

1. INTRODUCTION

Nonequilibrium molecular dynamics simulations of planar Couette flow using the SLLOD algorithm[1,2] have successfully predicted non-Newtonian viscosity, pressure, and normal stress difference as a function of shear rate. The SLLOD algorithm correctly incorporates the external shearing field which prevents the attainment of an equilibrium state by maintaining a constant velocity gradient. This external field continuously performs work on the system, and the resulting heat is removed or added using the Gaussian isokinetic constraint, so that a nonequilibrium steady state can be achieved.

Recently there has been an emphasis toward the better characterization of the nonequilibrium steady state using the description offered by fractal analysis. In simple terms, stationary nonequilibrium flows develop by generating "multifractal" strange attractor objects of zero volume in the

[1] Department of Physics, University of NSW, University College, ADFA, Canberra, ACT 2600, Australia. dji@phadfa.ph.adfa.oz.au.
[2] School of Physics, University of NSW, Kensington, NSW 2033, Australia.

0022-4715/94/0800-1045$07.00/0

phase space available to the system. One way to study the phase space contraction is through the Lyapunov spectrum of the steady-state flow. The Lyapunov exponents describe the time-averaged rates of expansion and contraction of a Lagrangian hypersphere made up of comoving phase space points. The principal axes of such a hypersphere grow, or shrink, exponentially fast with time, and the corresponding set of phase space growth and decay rates is called the Lyapunov spectrum. For dissipative systems the sum of Lyapunov exponents is negative and gives the rate of the phase space volume contraction. This method was used to quantify the phase space contraction for a one-dimensional conductivity of a particle in a periodic potential,[3] the soft-disk shear flow obeying SLLOD equations of motion,[4,5] boundary-driven shear flow with thermostatted boundaries,[6] and color diffusion.[7,8] The information dimension of the attractor representing the steady state can then be found using the Kaplan–Yorke conjecture.[9] The Lyapunov spectrum approach was favored because it has been linked to the transport coefficients[4,7] and combined with the sum rule[5] could provide an alternative method for calculations of viscosity in thermostatted sheared systems.

Alternatively, the generalized dimensions of an attractor can be found using basic algorithms which in the end reduce their calculations to elementary box counting. This approach becomes prohibitively expensive for systems with even a few (more than 4) degrees of freedom, and therefore only the simplest systems have been characterized: color diffusion in the two-dimensional Lorentz gas[10] and planar two-body Couette flow.[11] The generalized dimensions of these attractors have been shown to decrease as the system is driven arbitrarily far from equilibrium because the behavior of the system becomes more ordered due to biasing by the shearing field. The "multifractal" form of the attractors is a consequence of the local variation of the fractal dimension in space.

In this paper we aim to characterize the attractor of the simplest sheared system, the hard-disk Lorentz gas, including an additional degree of freedom which enters the picture as the consequence of the system being nonautonomous.

2. THE SYSTEM

The simplest nontrivial shearing system is one of two hard disks obeying the SLLOD equations with periodic "sliding brick"[1,2,12] boundary conditions. This system can be viewed from a frame fixed in space, or alternatively from a frame fixed on one of the particles. In the latter case, one of the particles can be regarded as a disk of radius σ forming a periodic lattice of scatterers, and the other is a point moving at velocity $\mathbf{v}_2 - \mathbf{v}_1$ (and the peculiar momentum $\mathbf{p} = \mathbf{p}_2 - \mathbf{p}_1$) and scattering throughout the periodic

lattice. Due to the moving periodic boundary conditions, the lattice of scatterers changes its symmetry periodically from triangular to rectangular. This is the Lorentz model of isothermal shear flow.[13]

The SLLOD equations for the two-body Lorentz system (with units of mass chosen so that the mass of the moving disk is equal to unity) read

$$\begin{aligned} \dot{x} &= p_x + \gamma y \\ \dot{y} &= p_y \\ \dot{p}_x &= F_x - \gamma p_y - \alpha p_x \\ \dot{p}_y &= F_y - \alpha p_y \end{aligned} \tag{1}$$

where $\mathbf{p} = \mathbf{p}_2 - \mathbf{p}_1$ is the relative momentum of the disks and $\mathbf{r} = (x, y)$ their relative position vector. The parameter γ is the shear rate ($\gamma = \partial u_x / \partial y$, where $\mathbf{u}$ is the streaming velocity) and α is the time-dependent Gaussian "friction coefficient" which ensures the conservation of the kinetic energy at all times,

$$\alpha(t) = (\mathbf{F} \cdot \mathbf{p} - \gamma p_x p_y)/p^2$$

$\mathbf{F}(\mathbf{r})$ is the force between the disks, and in the case of hard disks it is zero for the distances $r > \sigma$ and infinitely repulsive for $r \leqslant \sigma$, where σ is the diameter of the disk.

The two-dimensional sheared Lorentz gas thus apparently has three degrees of freedom because the center of mass, kinetic energy, and the total momentum are the constants of motion. The degrees of freedom for the hard-disk sheared Lorentz system are conventionally chosen as the position coordinates of the point particle (x, y) and the polar angle θ of the relative momentum $\mathbf{p}$ with respect to the x axis. Between the collisions there is no interaction $\mathbf{F}$ between disks and the SLLOD equations reduce to

$$\begin{aligned} \dot{\theta} &= \gamma \sin^2 \theta \\ \dot{x} &= p \cos \theta + \gamma y \\ \dot{y} &= p \sin \theta \end{aligned} \tag{2}$$

and they can be solved analytically to give[13]

$$\begin{aligned} \cot \theta(t) &= \cot \theta_0 - \gamma t \\ x(t) &= x_0 + y_0 \gamma t - \frac{p}{\gamma} \cot \theta \ln \frac{\tan(\theta/2)}{\tan(\theta_0/2)} - \frac{2p}{\gamma} \left(\frac{1}{\sin \theta} - \frac{1}{\sin \theta_0} \right) \\ y(t) &= y_0 + \frac{p}{\gamma} \ln \frac{\tan(\theta/2)}{\tan(\theta_0/2)} \end{aligned} \tag{3}$$

However, there is an additional motion which we need to specify in order to be able to reproduce the behavior of the system, and that is the relative motion of the neighboring scatterers as measured by the position Δ of those scatterers (see Fig. 1)

$$\Delta(t) = \mathrm{mod}(\Delta_0 + \gamma L t, L) \tag{4}$$

The equations of motion (1) are nonautonomous through the use of periodic boundary conditions in the simulation program: the introduction of the new variable Δ allows Eqs. (1) to be transformed into an autonomous set. Thus the system has four degrees of freedom and therefore the attractor is embedded in four-dimensional space. The four variables can be chosen as the distance of the point particle from the center r, the polar angle of the position β, the direction of the relative momentum θ, and the position of the neighbours Δ (see Fig. 1). In previous calculations of the generalized dimensions of this system[4,5,11] the variable Δ was ignored, i.e., it was assumed that the probability of the collisions would not depend on the position of the neighbors in the case of purely repulsive potentials with a cutoff.[4] That assumption was justified by the fact the particle does not interact with particles in the neighboring periodic cells, that Δ does not explicitly depend on any of the other phase space variables, and that its time dependence is piecewise linear. It was nevertheless recognized by Hoover *et al.*[6,10,14] that periodic time dependence of the planar shear flow should be taken into account. We propose to show that Δ is indeed a rele-

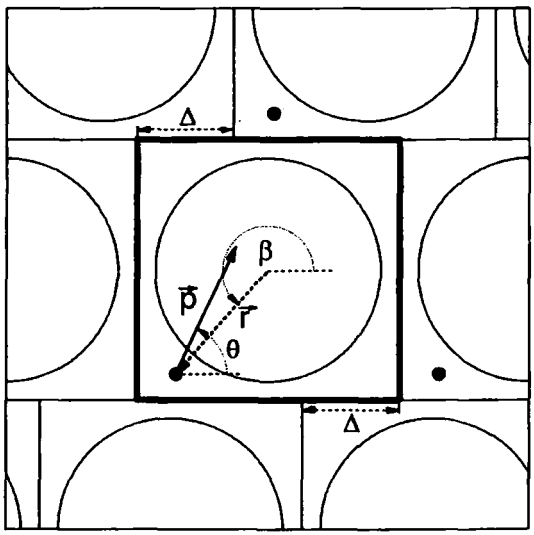

Fig. 1. Definition of phase space variables.

vant variable, that the explicit periodic time dependence it induces in the system causes some *synchronization of collisions* with the certain positions of the neighbors Δ, so that the resulting fractal dimension of the attractor is not simply larger by 1 than the dimension with Δ ignored.

3. THE COLLISIONS

In Eq. (1) the collisional momentum transfer is complicated by the isothermal restriction. In the equation for the rate of change of momentum, the term which causes the momentum change of an isokinetic system is nonlocal, depending both on position and momentum itself. An exact method for solving this type of collision in the limit when the force between the particles goes to infinity was described by Kratky and Hoover[15] for the Evans–Gillan equations of heat flow. In our approach the constant force is allowed to increase to infinity, causing the time of collision ε (while the point particle is inside the scatterer) to go to zero, keeping the product $F\varepsilon$ finite. The length of the infinitely short time interval ε is determined by the condition that the distance of the point particle to the origin of the scatterer at the beginning and at the end of the collision has to be equal to σ.

Using this criterion in Eq. (1) gives the momentum $\mathbf{p}_f$ after the collision both in the equilibrium and in the sheared isokinetic case.

3.1. Equilibrium Case

Let us compare the equilibrium isoenergetic and isokinetic scatterings of a point particle by a constant radial repulsive force $\mathbf{F}$ acting only within a sphere of radius σ.

In the isoenergetic case the magnitude of the momentum changes within the field as a part of the kinetic energy is converted into potential energy and vice versa, but the total energy is conserved. If the scattering is isokinetic, the momentum is not allowed to change its magnitude, only its direction. The equations of motion for the two cases are

Isoenergetic	Isokinetic
$\dot{x} = p_x$	$\dot{x} = p_x$
$\dot{y} = p_y$	$\dot{y} = p_y$
$\dot{p}_x = F\dfrac{x}{r}$	$\dot{p}_x = F\dfrac{x}{r} - \dfrac{\mathbf{F}\cdot\mathbf{p}}{p^2}p_x$
$\dot{p}_y = F\dfrac{y}{r}$	$\dot{p}_y = F\dfrac{y}{r} - \dfrac{\mathbf{F}\cdot\mathbf{p}}{p^2}p_y$

(5)

Although the equations of motion for the isokinetic collision are quite different from the ones in the conventional isoenergetic case, the isoenergetic and isokinetic trajectories of point particles calculated from the equations of motion in the constant radial repulsive field coincide in the hard-disk limit (as $F \to \infty$). We shall prove this result below.

The time ε the point particle spends inside the repulsive field depends on the strength of the field F and the initial momentum of the particle $\mathbf{p}_i$. We assume that in the hard-disk limit, i.e., when $F \to \infty$, the time $\varepsilon(F, \mathbf{p}_i) \to 0$ in such a way that the product $F\varepsilon(F, \mathbf{p}_i)$ stays finite,

$$\lim_{F \to \infty} F \cdot \varepsilon(F, \mathbf{p}_i) = A(\mathbf{p}_i) < \infty \tag{6}$$

Within the infinitely small time $\varepsilon(F, \mathbf{p}_i)$ the momentum changes from its initial value $\mathbf{p}_i$ to the final value $\mathbf{p}_f$. We shall look at the change of the radial component of the momentum p_r from p_{ri} to p_{rf} and tangential component p_t from p_{ti} to p_{tf} during the isokinetic collision. The equations of motion for the radial and tangential components of the momentum are

$$\begin{aligned} \dot{p}_r &= F\left(1 - \frac{p_r^2}{p^2}\right) + \frac{p^2}{r} - \frac{\dot{r}}{r} p_r \\ \dot{p}_t &= -\frac{F}{p^2} p_r p_t - \frac{\dot{r}}{r} p_t \end{aligned} \tag{7}$$

where $r = (x^2 + y^2)^{1/2}$. If the particle enters the repulsive field at the time ε_1 and leaves at time $\varepsilon_2 = \varepsilon_1 + \varepsilon(F, \mathbf{p}_{ri})$, the equations of motion (7) have to be integrated over the time interval ε. We are looking for the solution in the limit when $F \to \infty$, $\varepsilon = \varepsilon_2 - \varepsilon_1 \to 0$, and in that limit the contribution of the terms which do not contain F can be neglected because the function under the integral is then finite and is integrated over an infinitely short time interval. Therefore, in the limit $F \to \infty$, $\varepsilon \to 0$ the evolutions of p_r and p_t are governed by the equations

$$\dot{p}_r = F\left(1 - \frac{p_r^2}{p^2}\right) \qquad \text{and} \qquad \dot{p}_t = -\frac{F}{p^2} p_r p_t$$

with solutions

$$p_r(t) = p \tanh(Ft/p) \qquad \text{and} \qquad p_t(t) = p/\cosh(Ft/p) \tag{8}$$

so that

$$p_r^2 + p_t^2 = p^2 = \text{const.}$$

In particular,

$$p_{ri} = p \tanh(F\varepsilon_1/p) \qquad p_{ti} = p/\cosh(F\varepsilon_1/p)$$
$$p_{rf} = p \tanh(F\varepsilon_2/p) \qquad p_{tf} = p/\cosh(F\varepsilon_2/p)$$

In the equilibrium case p_r is also equal to the radial velocity in the system of units where $m = 1$. The condition on the integration time ε is that the total change of the distance from the center must be zero, i.e., the particle must leave the circular region of the repulsive field at the same radial distance as it had entered it. This means that the area under the $p_r(t)$ function in the interval $(\varepsilon_1, \varepsilon_2)$ must equal zero

$$\Delta r = \int_{\varepsilon_1}^{\varepsilon_2} p_r(t)\, dt \tag{9}$$

which has a nontrivial solution $\varepsilon_1 = -\varepsilon_2$, $p_{rf} = -p_{ri}$ and the total change in the radial component of the momentum is $\Delta p_r = -2p_{ri}$ just as in the isoenergetic case.

3.2. Sheared Case

To find the solutions for the isokinetic collisions of the Lorentz gas we have to solve the set of SLLOD equations (1) for the constant radial repulsive field F in the limit $F \to \infty$ at finite values of γ. Here the time spent within the field F depends not only on the initial radial component of the momentum p_{ri}, but also on the polar angle β of the collision. The product $F\varepsilon(F, p_{ri}, \beta)$ still stays finite in the hard-disk limit $(F \to \infty, \varepsilon \to 0)$.

Again, let us consider the rate of change of the radial and tangential components of the momentum,

$$\begin{aligned} \dot{p}_r &= F\left(1 - \frac{p_r^2}{p^2}\right) + \frac{\gamma p_x p_y}{p^2} p_r - \gamma p_t + \frac{p^2}{r} - p_r \frac{\dot{r}}{r} \\ \dot{p}_t &= -F \frac{p_r p_t}{p^2} + \gamma p_y \frac{y}{r} + \frac{\gamma p_x p_y}{p^2} p_t - p_t \frac{\dot{r}}{r} \end{aligned} \tag{10}$$

In the limit $F \to \infty$, $\varepsilon \to 0$ the terms which do not contain F can again be neglected. This means that during a hard-disk collision with shear the momentum obeys the same differential equations (8) as in the equilibrium case, only with different boundary conditions. The condition which gives us the value of $p_{rf} = p_r(\varepsilon_2)$ is given by (9), with the radial velocity no longer equal to the radial momentum, but rather

$$\dot{r} = p_r + \gamma xy/r \tag{11}$$

In the hard-disk limit the collision happens at one point at the distance $r=\sigma$ from the center, and $\gamma xy/r$ becomes a constant $\gamma x_0 y_0/\sigma$, where x_0 and y_0 are the coordinates of the point of collision ($x_0^2+y_0^2=\sigma^2$). The condition (9) now becomes

$$\int_{\varepsilon_1}^{\varepsilon_2}\left[p\tanh\left(\frac{Ft}{p}\right)+\frac{\gamma x_0 y_0}{\sigma}\right]dt=0$$

and the shaded areas above and under the curve on Fig. 2 must be equal. This gives an implicit equation for p_{rf},

$$\ln\left(\frac{1-p_{rf}^2/p^2}{1-p_{ri}^2/p^2}\right)=\frac{\gamma x_0 y_0}{\sigma p}\ln\left[\left(\frac{1+p_{rf}/p}{1-p_{rf}/p}\right)\left(\frac{1-p_{ri}/p}{1+p_{ri}/p}\right)\right] \tag{12}$$

The momentum after the collision can be evaluated from (12) numerically. In the limit $\gamma\to 0$ the right-hand side of Eq. (12) vanishes and p_{rf} reduces to the equilibrium solution. Also, the solution of (12) is obviously symmetric to time reversal, as is required of the solution to SLLOD equations. The described method for finding the momentum after a hard-disk collision can easily be generalized to three dimensions and it can be used also for systems with more particles if one assumes that there is only one collision happening at each instant.

The benefits of the hard-disk approximation are, apart from describing the exact limiting behavior, in the increased speed of calculations, although the hard-spring or repulsive WCA potentials give a more realistic picture. The solution is obtained only as a numerical solution of the algebraic equation $r=\sigma$, but it is nevertheless about 50 times faster than the previous

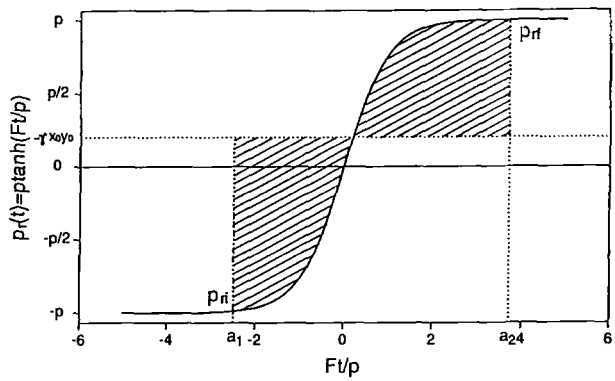

Fig. 2. Isokinetic collision with shear: the shaded area under the $\gamma x_0 y_0$ line must equal the shaded area above it ($a_1=F\varepsilon_1/p$ and $a_2=F\varepsilon_2/p$).

numerical integration of the SLLOD equations using a stiff repulsive potential, and is more suitable for the calculations where one has to evaluate the trajectory through a large number of collisions.

3.3. The Limitations of the Hard-Disk Approximation

The limitations of this method are that the infinite hard disks collide and separate only for $\gamma\sigma/p \leqslant 2$. For larger shear rates $\sigma\gamma/p > 2$ the point particle remains with the scatterer if it hits it at certain values of angle β, due to the strong shearing field across the cross section of the scatterer. This behavior for $\gamma\sigma/p > 2$ can be found from the following argument: if the particle is to bounce off after a collision, its radial velocity after the collision must be positive. In other words, for every angle β at collision there must exist an angle θ such that the inequality

$$\dot{r}(\theta, \beta)|_{r=\sigma} > 0 \tag{13}$$

can be satisfied. Figures 3a and 3b show the (θ, β) plane at the collision, where $r = \sigma$. In the gray regions $\dot{r} < 0$, and in the white regions $\dot{r} > 0$. The hard-disk collision represents a mapping of points in gray regions with $\dot{r} < 0$ onto white regions with $\dot{r} > 0$ *along a horizontal line*, because during a hard-disk collision the position of a particle on the circumference of the scattering disk is not allowed to change. When $\gamma\sigma/p \leqslant 2$ (Fig. 3a) every point in the gray region can be mapped on some point in the white region *along a horizontal line*. When $\gamma\sigma/p > 2$ there exist intervals of β (shaded on Fig. 3b) such that *all corresponding angles* θ give $\dot{r} < 0$. If a point particle

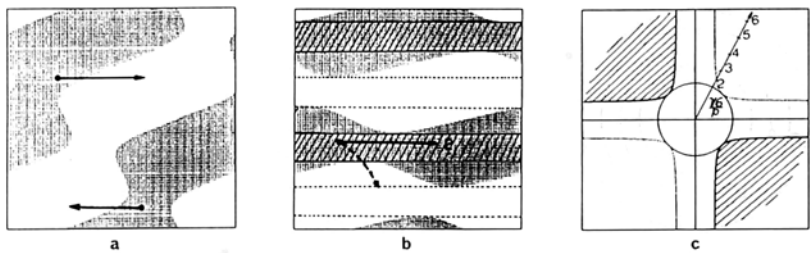

Fig. 3. (a, b) The hard-disk collision as a mapping in the (θ, β) plane for $\gamma\sigma/p = 1.5$ and $\gamma\sigma/p = 3$, respectively. The angle $\theta \in [0, 2\pi]$ is on the abscissa and the ordinate is $\beta \in [0, 2\pi]$. The mapping goes horizontally from the gray regions where $\dot{r} < 0$ to white regions where $\dot{r} > 0$. *Forbidden* collisions are in the shaded parts of the gray regions. (c) The dependence of the *forbidden* β intervals on $\gamma\sigma/p$ in polar coordinates: $\gamma\sigma/p$ is the polar axis and β is the angular variable. Forbidden angles β for $\gamma\sigma/p > 2$ are in the shaded area. The symmetric area enclosed by the dotted lines represents values of β in which collisions cannot occur.

collides with the scatterer at an angle β from this interval, it cannot bounce off. If, on the other hand, the interaction potential between the particles is very steep but smooth, the point particle can still penetrate the scatterer infinitesimally and "slide through," exiting in an allowed interval of β (dashed line on Fig. 3b). There are also intervals of β where $\dot{r} > 0$ for every θ and the collisions cannot occur (between the dotted lines on Fig. 3b). These effects can be seen if we look at the probability distributions of the angle β at $r = \sigma$ at the beginning and at the end of collision for soft disks: for $\gamma\sigma/p > 2$ these distributions differ considerably, the former having zero probability at the "impossible" intervals and the latter showing zero probability at the "forbidden" intervals. The dependence of the lengths of "forbidden" and "impossible" β intervals on $\gamma\sigma/p$ is shown on Fig. 3c.

4. PROBABILITY DISTRIBUTIONS

The probability distributions for variables θ, β, and Δ at $r = \sigma$, i.e., at the collision, are shown on Fig. 4 for four different values of shear rate $\gamma\sigma/p$. The distributions were evaluated for the reduced density of $\rho\sigma^2 = 0.4$ after 1.5 million collisions. The distribution of the angle θ before the collision becomes more nonuniform as the shear rate increases, showing more localized values of θ with the peaks closer to $\theta = 0$ and $\theta = \pi$ favored as the γt term plays a more important role in Eq. (3) for larger $\gamma\sigma/p$ values. The peak of the distribution of the angle of collision β also becomes more pronounced and moves toward the asymptote of $+\pi/2$ as the point particle moves more horizontally at larger γ values due to larger streaming velocity. The distribution of θ after the collision more closely resembles the distribution of β as the momentum after the most probable collisions (for β in second and fourth quadrants) becomes almost radial (see Fig. 2). Not only do the angular distributions of β and θ before and after the collision become highly nonuniform due to the shear-induced biasing, but also the distribution for Δ shows heavily populated peaks for moderately sheared systems ($\gamma\sigma/p > 0.75$). This shows that the collisions "favor" certain Δ positions in that the collisions become synchronized with the periodic change of symmetry of the scatterers' positions as the shear rate increases. This result prompted a more detailed study of the correlation between Δ and x, y, and θ at collisions.

5. POINCARÉ SECTIONS OF THE ATTRACTOR

Because the trajectory in phase space between the collisions is piecewise smooth, we can eliminate one of the dimensions in our four-dimensional phase space by looking at the density of points at the intersection of the

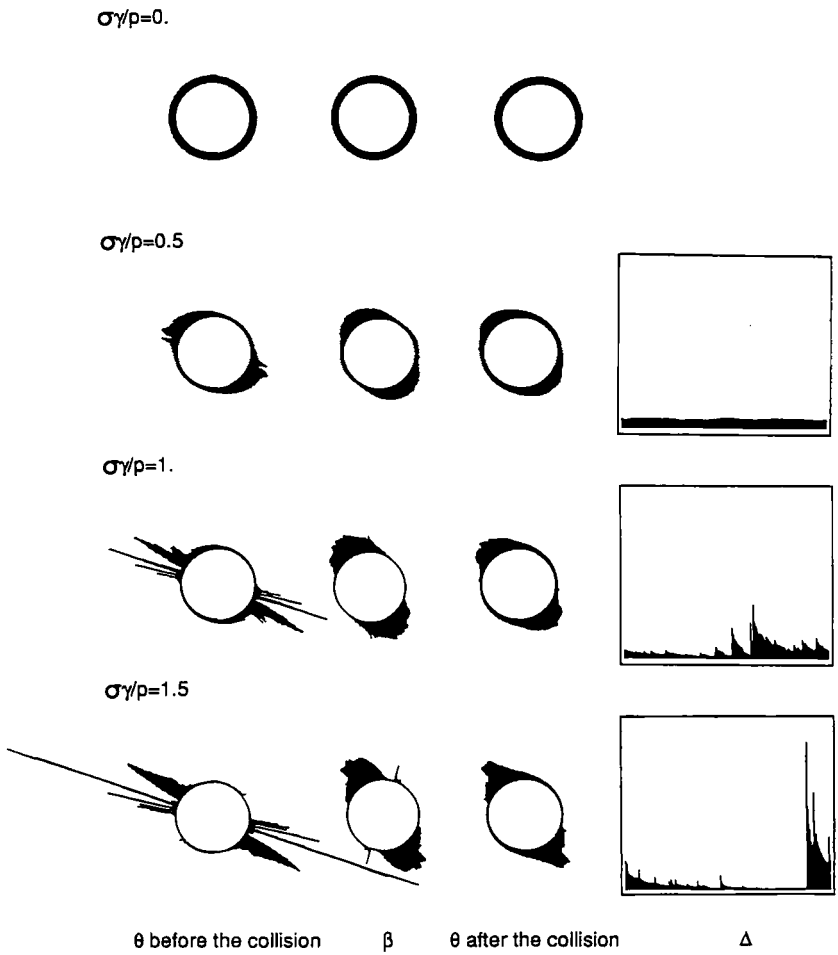

Fig. 4. Probability distributions for each of the phase space variables at the collision ($r = \sigma$) in arbitrary units. The angular distributions are shown on the circumference of a unit circle to emphasize their periodicity; the range of variable Δ is between 0 and L.

attractor and some three-dimensional hyperplane. The resulting Poincaré section is now embedded in *three-dimensional* space and so is easier to visualize.

The easiest cross section to find is that at $r = \sigma$, which consists of points defined by triplets (θ, β, Δ), i.e., the direction of momentum, position of the point particle, and position of the neighboring cells at the time of the collision. During the collision the momentum changes its direction discontinuously from θ (before the collision, where $\dot{r} < 0$) to θ' (after the collision,

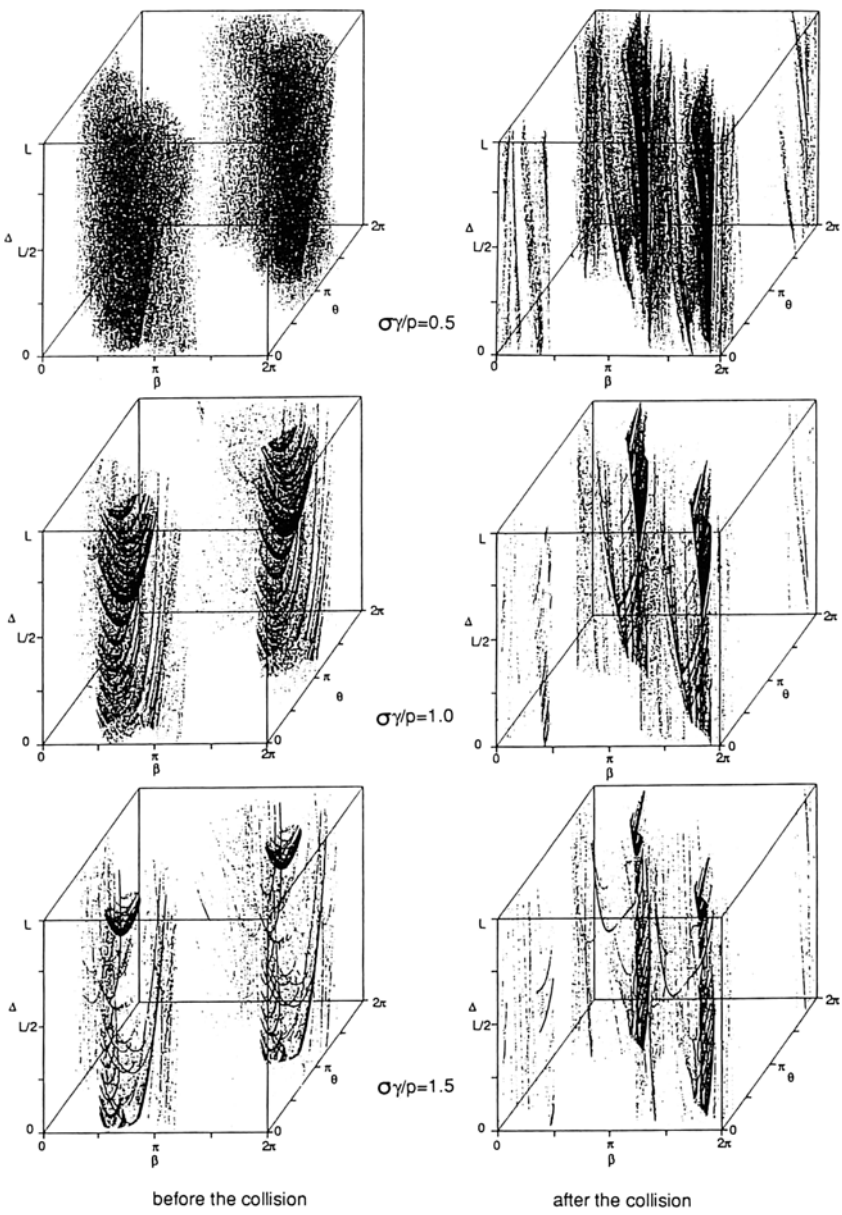

Fig. 5. Three-dimensional one-sided Poincaré sections of the attractor at $r \approx \sigma$ for different values of the parameter $\gamma\sigma/p$.

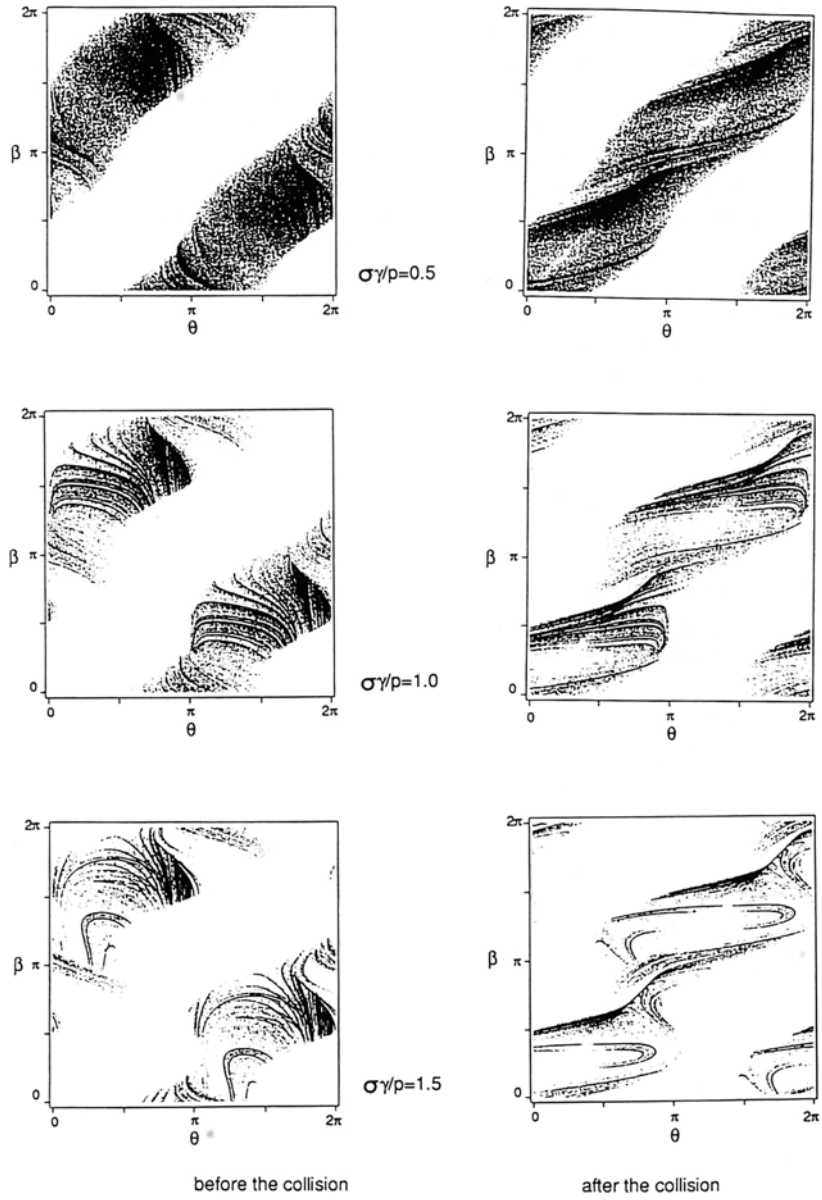

Fig. 6. Projections of the Poincaré sections from Fig. 5 onto the (θ, β) plane.

where $\dot{r} > 0$), so that the collision itself can be considered to introduce a mapping from a set of points (θ, β, Δ) at $r = \sigma$ before the collision (with $\dot{r} < 0$) to the set of points (θ', β, Δ) at $r = \sigma$ after the collision (with $\dot{r} > 0$). The two sets of points are one-sided Poincaré sections. These precollision and postcollision Poincaré sections, each containing a time series of 250,000 points, are shown on Fig. 5 for three different values of $\gamma\sigma/p$. The attractor for the sheared Lorentz gas system is a four-dimensional object which consists of piecewise smooth trajectories in phase space starting from a set of points (θ', β, Δ) at $r = \sigma$ with $\dot{r} > 0$ and finishing at the set of points (θ, β, Δ) at $r = \sigma$ with $\dot{r} < 0$ before the next collision.

If all values Δ were equally probable for all collisions, the point clouds of the Poincaré sections would have the same density throughout the range of Δ values. However, the plots in Fig. 5 unmistakably show correlations between the angular variables and Δ. In addition these correlations strengthen as $\gamma\sigma/p$ increases from 0.5 to 1.5.

Closer inspection of the detailed layering in the precollision Poincaré section for $\gamma\sigma/p = 1$ reveals the dependence of (θ, β) on Δ. Indeed from Fig. 4 it can be seen that the density of points in the Poincaré cloud changes according to the Δ value. An examination of the precollision sections of Fig. 5 gives the actual stratification of this effect as the cloud density changes through (θ, β, Δ) values. The Δ dependence of the precollision cloud is quite complicated, but the pattern at different Δ layers is sufficiently different to associate these pattern changes with different types of collisions (θ, β) occurring at different Δ. Consequently the average interval between certain types (θ, β) of collisions becomes commensurable with the period of the symmetry change of the scatterers' positions with increasing shear rate. Thus Δ is an important a degree of freedom, as much as the polar angles θ and β.

6. CORRELATION DIMENSION OF THE ATTRACTOR

The correlation function measuring the spatial correlation of n points in a point cloud is defined as the fraction of pairs of points whose relative distance is less than ε,

$$C(\varepsilon) = \lim_{n \to \infty} \frac{1}{n^2} \sum_{i,j=1}^{n} H(\varepsilon - |\mathbf{r}_i - \mathbf{r}_j|) \tag{14}$$

Here H is the Heaviside step function, $H(x) = 0$ if $x < 0$ and 1 if $x \geqslant 0$. The correlation dimension ν is the exponent defining the critical behavior of correlation function for small ε,[16]

$$C(\varepsilon) = \varepsilon^{-\nu} \tag{15}$$

For small ε the graph of $\log C(\varepsilon)$ vs. $\log \varepsilon$ becomes linear, and ν can be found as the slope of the line. When Eq. (14) is used to measure the correlation dimension of an attractor, the points $\mathbf{r}_i$ on the attractor are chosen at random according to the probability density associated with the attractor. The vectors $\mathbf{r}_i$ are then the positions of points in phase space (*not* configurational space). An efficient algorithm[16] was used to calculate the correlation dimension on a Connection Machine CM-2. In our case the points in (14) are the points on the precollisional or postcollisional Poincaré sections found from a single trajectory, and vectors $\mathbf{r}_i$ represent the triplets (θ, β, Δ) at $r = \sigma$ just before or after the collision. A resolution for ε between 2^{-6} and 2^{-15} was given by the evaluation of the coordinates (θ, β, Δ) for 2^{19} collisions. A box-counting algorithm for the fractal dimension (capacity) required an estimated 2^{28} collisions for the maximal resolution of 2^{-8}.[10] The correlation dimension depends on the density of the points on the attractor. If the phase space is divided into N bins of side length ε, a definition of ν equivalent to (15) can be obtained in terms of the probability of visiting these different bins by a typical trajectory when the grid is refined in the limit,

$$\nu = \lim_{\varepsilon \to 0} \frac{\ln \sum_{i=1}^{N} P_i^2}{\ln \varepsilon} \tag{16}$$

where N is the total number of bins and P_i is the probability of the ith bin being visited. Definitions (15) and (16) are entirely equivalent.

We found the correlation dimension of the Poincaré sections before and after the collision and the results are shown on Fig. 7. On the attractor, the points of the two Poincaré sections are connected by piecewise

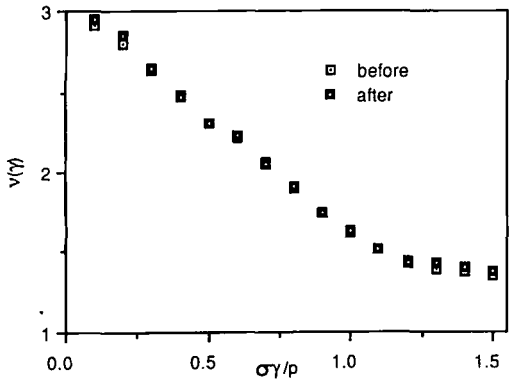

Fig. 7. Dependence of the correlation dimension of the Poincaré section before and after the collision on shear rate.

smooth trajectories representing the behavior between the collisions, which means that the difference between the correlation dimension of the whole attractor and the correlation dimension of the Poincaré section should be close to unity. Also, because the time dependence of the system between the collisions is analytic (except for the discontinuities due to boundary crossings) and because the system is deterministic, i.e., the number of points in the Poincaré sections is conserved, we expect the dimensions of the two sections to be the same. The results show the dimensional contraction of the attractor with the increase of shear rate, from 4 very close to equilibrium ($\gamma\sigma/p = 0$) to less than 2.5 for $\gamma\sigma/p > 1$. The limiting value of the dimension of the attractor as $\gamma \to 0$ is 4, but in reality the equilibrium value cannot exceed 3 because in that case Δ is constant. The limiting value of 4 can then be interpreted as the dimension of a set of two-dimensional Poincaré sections corresponding to all possible configurations of the scatterers' lattice, i.e., to all possible values of Δ.

The importance of Δ can be summarized from the projection of all points of the Poincaré sections of Fig. 5 onto the (θ, β) plane (see Fig. 6). This gives the Poincaré section of the Lorentz gas attractor with Δ completely ignored. The results for the full three-dimensional Poincaré sections and the projections are compared on Fig. 8. With no correlation between the collisions and Δ, the difference between the two correlation dimensions would be unity, as it is for shear rate approaching zero. But as $\sigma\gamma/p$ increases, the difference decreases such that for the Poincaré sections before the collision (Fig. 8a) the two dimensions coincide when the dimension of the full Poincaré section becomes less than 2. The reason for this can be seen from the following: if the dimension is less than 2, points of the observed set (at least to the given resolution) lie on a collection of lines rather than a surface in three-dimensional space. The projection is then also a set of lines provided the lines are not perpendicular to the plane of projection.

After the collision the difference between the dimensions of the Poincaré section and its projection decreases below unity with the increasing shear rate, but beyond $\sigma\gamma/p = 0.75$ that difference is remarkably constant (Fig. 8b). This can be qualitatively explained from the collision law for hard disks: if the collisions occur in the second or fourth quadrant, where they are the most probable, then the expression γxy is positive, which pushes the direction of final momentum toward radial (see Fig. 5). Thus as $\sigma\gamma/p$ increases, a larger fraction of the collisions having initial momenta at the same angle β come out of the collision nearly radially and are counted in the same two-dimensional bin of the projection after the collision. But if we include the Δ axis in the coordinate system, we find that the points that fall into the same bin in the projection are found in cubes with dif-

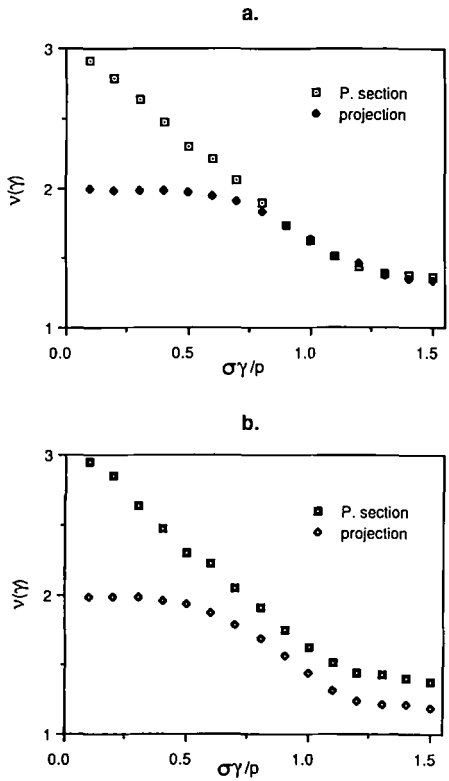

Fig. 8. Correlation dimension of the Poincaré section and its projection onto the (θ, β) plane (a) before and (b) after the collision.

ferent Δ, i.e., some "lines" of the Poincaré section after the collision are nearly perpendicular to the projection plane. Thus, the difference between the correlation dimensions of the projections before and after the collision increases with the shear rate (Fig. 9). The trajectories associated with the projection of the Lorentz gas attractor onto the three-dimensional phase space (with Δ ignored) start from an object of lower dimension (projection after the collision) and end on an object of higher dimension (projection before the collision). If the dimension of the Poincaré sections is to be conserved throughout the attractor, it is necessary to include the additional degree of freedom Δ.

Figure 9 also shows the γ dependence of the correlation dimension for a soft-disk Lorentz system studied by Morriss.[11] He calculated a sequence of generalized dimensions for the projection of the attractor onto a three-

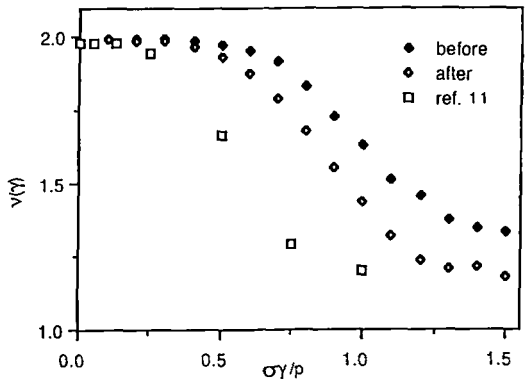

Fig. 9. Comparison of the correlation dimensions of the projections before and after the collisions with the correlation dimensions from ref. 11.

dimensional phase space (ignoring Δ) using a box-counting algorithm for a collection of points on the phase space trajectory separated by a small time interval dt. His correlation dimension less unity should be close to our correlation dimension of the projection. In fact, it becomes less as the shear rate increases. We attribute the difference partly to the use of the relatively soft WCA potential in Morriss' work, and partly to the nonuniform "natural measure"[9] along the trajectory, which might result in the correlation dimension of the piecewise smooth line being less than unity because of the probabilistic nature of the correlation dimension.

7. CONCLUSION

The results presented here show that the correlation dimension of the attractor for the two hard-disk sheared system, when properly embedded in four-dimensional phase space, decreases with shear rate from 4 (close to equilibrium) to a value between 2 and 2.5 for $\gamma\sigma/p > 2$. It also shows that it is necessary to include a degree of freedom representing the explicit periodic time dependence of the flow to get a proper description of the system. One can get an idea of the role the mechanism of the sheared thermostatted collisions plays in the collapse of the visited phase space on the strange attractor of zero volume by the following considerations: if we start with $\Delta = 0$ and a uniform distribution of points in the (θ, β) plane before the collision, these are mapped by the law (11) onto a highly nonuniform distribution after the collision, where the previously homogeneous regions are squeezed, stretched, and overlapped, as expected. Such a nonuniform distribution of angles θ and β serves as a set of initial conditions for the

trajectories between the collisions, ending in a nonuniform distribution before the collision. At this point the periodic time dependence of the moving boundary conditions enters the picture. The points are then again mapped onto the region $\dot{r} > 0$ with increasing inhomogeneity at each step, until a pattern similar to Fig. 6 is obtained. After a large sequence of such mappings and evolutions have taken place, the fraction of the types of the collisions (increasing with the shear rate) which can be differentiated at a given precision will be on average periodic, with the average period commensurate with $1/\gamma$, thus forming a beginning of a "devil's staircase" (see, e.g., ref. 17). In that case both the collisions and the moving boundary conditions would be responsible for the formation of the attractor.

ACKNOWLEDGMENTS

We would like to thank the computer centre at the Australian National University for the generous grant of computer time on the Connection Machine CM-2.

REFERENCES

1. D. J. Evans and G. P. Morriss, *Phys. Rev. A* **30**:1528 (1984).
2. D. J. Evans and G. P. Morriss, *Comp. Phys. Rep.* **1**:297 (1984).
3. B. Holian, W. G. Hoover, and H. A. Posch, *Phys. Rev. Lett.* **59**:10 (1987); W. G. Hoover *et al.*, *Mol. Simul.* **1**:79 (1987).
4. G. P. Morriss, *Phys. Rev. A* **37**:2188 (1988).
5. D. J. Evans, E. G. D. Cohen, and G. P. Morriss, *Phys. Rev. A* **42**:5990 (1990).
6. H. A. Posch and W. G. Hoover, *Phys. Rev. A* **39**:2175 (1989).
7. W. G. Hoover and H. A. Posch, *Phys. Lett.* **123A**:227 (1987).
8. H. A. Posch and W. G. Hoover, *Phys. Rev. A* **38**:473 (1988).
9. J. D. Farmer, E. Ott, and A. Yorke, *Physica* **7D**:153 (1983).
10. W. G. Hoover and B. Moran, *Phys. Rev. A* **40**:5319 (1989).
11. G. P. Morriss, *Phys. Rev. A* **39**:4811 (1989).
12. A. W. Lees and S. F. Edwards, *J. Phys. Chem.* **5**:1921 (1972).
13. J. C. Ladd and W. G. Hoover, *J. Stat. Phys.* **38**:973 (1985).
14. W. G. Hoover and B. Moran, *Chaos* **2**:599 (1992).
15. W. G. Hoover and K. W. Kratky, *J. Stat. Phys.* **42**:1103 (1986); K. W. Kratky and W. G. Hoover, *J. Stat. Phys.* **48**:873 (1987).
16. P. Grassberger and I. Procaccia, *Phys. Rev. Lett.* **50**:346 (1983).
17. P. Berge, Y. Pomeau, and C. Vidal, *L'Ordre Dans le Chaos* (Hermann, Paris, 1984).